How Uncertainty in Field Measurements of Ice Nucleating Particles Influences Modeled Cloud Forcing

S. GARIMELLA, D. A. ROTHENBERG, M. J. WOLF, AND C. WANG

Department of Earth, Atmospheric and Planetary Sciences, Massachusetts Institute of Technology, Cambridge, Massachusetts

D. J. CZICZO

Department of Earth, Atmospheric and Planetary Sciences, and Department of Civil and Environmental Engineering, Massachusetts Institute of Technology, Cambridge, Massachusetts

(Manuscript received 25 March 2017, in final form 11 October 2017)

ABSTRACT

Field and laboratory measurements using continuous flow diffusion chambers (CFDCs) have been used to construct parameterizations of the number of ice nucleating particles (INPs) in mixed-phase and completely glaciated clouds in weather and climate models. Because of flow nonidealities, CFDC measurements are subject to systematic low biases. Here, the authors investigate the effects of this undercounting bias on simulated cloud forcing in a global climate model. The authors assess the influence of measurement variability by constructing a stochastic parameterization framework to endogenize measurement uncertainty. The authors find that simulated anthropogenic longwave ice-bearing cloud forcing in a global climate model can vary up to 0.8 W m^{-2} and can change sign from positive to negative within the experimentally constrained bias range. Considering the variability in the undercounting bias, in a range consistent with recent experiments, leads to a larger negative cloud forcing than that when the variability is ignored and only a constant bias is assumed.

1. Introduction

Atmospheric ice nucleation proceeds via a variety of pathways. Homogeneous nucleation occurs when ice crystals grow from clusters of water molecules formed from an aqueous phase (Pruppacher and Klett 1997). Such nucleation is only favorable in atmospheres colder than −38°C with water activities close to unity (Koop et al. 2000). Processes of heterogeneous nucleation occur when an ice nucleating particle's (INP's) surface lowers the energy barrier of ice formation and can occur at temperatures lower than 0°C and any saturation in excess of that of water ice (Pruppacher and Klett 1997). Deposition freezing occurs in air supersaturated with respect to ice when water vapor nucleates onto the INP surface directly as solid ice (Lynch et al. 2002). An INP can also nucleate the ice phase from within an aqueous capsule, a process known as immersion or condensation freezing (Murray et al. 2012).

INPs therefore play an important role in the climate system by forming ice clouds and thus influencing cloud albedo, precipitation, and radiative transfer (Storelvmo et al. 2011; Lau and Wu 2007; Forster et al. 2007). Despite their importance, there are significant uncertainties in field measurements of INP concentrations because of the complexities of atmospheric ice nucleation processes (Boucher et al. 2013). Field measurements over the last few decades with continuous flow diffusion chamber (CFDC) INP counters (e.g., DeMott et al. 2003a,b; Chou et al. 2011; Boose et al. 2016) have been used to constrain INP concentrations, and these have been used to build parameterizations used in climate models. INP concentrations have then been used with various secondary and ice multiplication processes to model ice crystal concentration as a function of temperature and particle concentration (DeMott et al. 2010, hereafter D10; Tobo et al. 2013; DeMott et al. 2015). Such parameterizations are used in both weather prediction models (Fan et al. 2014; Hande et al. 2015) and global climate models (Storelvmo et al. 2011; Xie et al. 2013; Tan and Storelvmo 2016), where the modeled cloud microphysical processes and cloud radiation have been shown to be sensitive to the ice nucleation parameterization.

Corresponding author: D. J. Cziczo, djcziczo@mit.edu

DOI: 10.1175/JAS-D-17-0089.1

CFDC measurements have been shown to be subject to a systematic low bias in reported INP concentrations because of nonideal instrument behavior (DeMott et al. 2015). DeMott et al. (2015) considered systemic instrumental biases with the Colorado State University (CSU) CFDC chamber and expanded on the work of Tobo et al. (2013) by proposing the addition of a ''calibration factor'' (cf) of 3 to multiply measured INP to provide a corrected value that best agreed with measured data. By definition, Tobo et al. (2013)—and all previous studies—assumed no bias (i.e., a factor of 1). More recently, Garimella et al. (2017) showed that in a commercial CFDC, the Spectrometer for Ice Nuclei (SPIN; Garimella et al. 2017), a constant correction factor did not capture the variability of the bias over that instrument's operational range.

It should be noted that the instrumental biases (due to, for example, particles spreading outside of the aerosol lamina) addressed here, as described by DeMott et al. (2015) and Garimella et al. (2017), are different than the measurement uncertainty associated with sample nonidealities or spatial and temporal differences. DeMott et al. (2003a,b) noted that CFDC instruments have a limited size range from which they can sample. D10 noted that the variability in their INP parameterization related to aerosol composition and sampling location and time. All of these factors result in measurement uncertainty, but they do not consider or account for the instrument biases considered here.

Taken together, DeMott et al. (2015) and Garimella et al. (2017) suggest that instrumental bias leads to a systematic underestimation of INP in both the deposition and immersion modes as well as confusion between deposition- and immersion-mode nucleation and droplet formation. There is additional observational evidence this bias exists when idealized and actual ice nucleation behavior are considered (Fig. 1). In an idealized case (Fig. 1a), an increase in deposition INP with increasing humidity is expected until water saturation, at which point all immersion INP activate (Wex et al. 2014; DeMott et al. 2015). In a realistic case (Fig. 1b), a perfect signal is not expected because of detector noise; a limit of detection (LOD) ''sets'' the lowest measurable INP concentration. The expected steady increase in the deposition INP with increasing humidity until liquid water saturation is reached is only apparent when the concentration exceeds the LOD. The step function behavior of immersion INP activating at water saturation is subdued because instrument nonidealities result in some particles not experiencing the maximum supersaturation present in the chamber (explained in more detail in the following paragraphs). As a result, a portion of the aerosol particles experience less than the maximum chamber saturation with respect to ice, and an underestimation of deposition INP is reported. Also as a consequence, some depositional ice nucleation is still occurring concurrent with immersion-mode nucleation by the fraction of particles experiencing the maximum chamber saturation. Confusion similarly exists since some immersion nucleation occurs concurrent with droplet formation at humidities exceeding liquid water saturation (Rogers 1988; Stetzer et al. 2008; Garimella et al. 2016). Note that reported CFDC data more closely resemble Fig. 1b than Fig. 1a (Garimella et al. 2017; DeMott et al. 2015).

Here, we consider the effect of this bias on simulated cloud radiative forcing using the National Center for Atmospheric Research Community Earth System Model, version 1.2.2, with the Community Atmosphere Model, version 5.3 (CAM5.3), run at 2° horizontal resolution. The model is an updated version of CAM5.0 described by Neale et al. (2010), including a newer cloud microphysics scheme (Gettelman et al. 2015), which is coupled with a detailed multimode, two-moment, mixing-state-resolving aerosol model (Kim et al. 2008, 2014). We refer to this coupled aerosol model as the Model of Aerosols for Research of Climate, version 1.0.2 (MARC).

2. Methodology

The effect of CFDC measurement bias on climate model–simulated cloud radiative forcing is investigated using CAM5-MARC. By default, MARC utilizes the ice nucleation scheme of Liu and Penner (2005), which includes a CFDC-based parameterization based on Eq. (2.4) of Meyers et al. (1992, hereafter MEY) to compute the heterogeneous ice nucleation in mixed-phase clouds (het ice) between 0° and −40°C. Mixed-phase clouds are taken to form only at (or above) water saturation, so the ice saturation ratio S_{ice} used by this scheme at a given temperature is the ratio of the saturation vapor pressure over liquid e_{liq} to the saturation vapor pressure over ice e_{ice} at that temperature; that is, $S_{\text{ice}}(T) = e_{\text{liq}}(T)/e_{\text{ice}}(T)$. In this study, the MEY parameterization is replaced by various versions of the more recent CFDC-based parameterization of D10, which take the form

$$n_{\text{INP}}(n_{\text{aer}>500}, T) = (\text{cf})a(273.16 - T)^b \times (n_{\text{aer}>500})^{[c(273.16-T)+d]}, \quad (1)$$

where n_{INP} is the number of INP; T is the temperature (K), and $n_{\text{aer}>500}$ is the number of aerosol particles larger than 500 nm; a, b, c, and d are empirically derived constants from D10; and cf is a constant or variable calibration factor. The base case (hereafter case B) is the D10 parameterization tuned to match satellite observations of longwave cloud forcing from the year 2000 from the Clouds

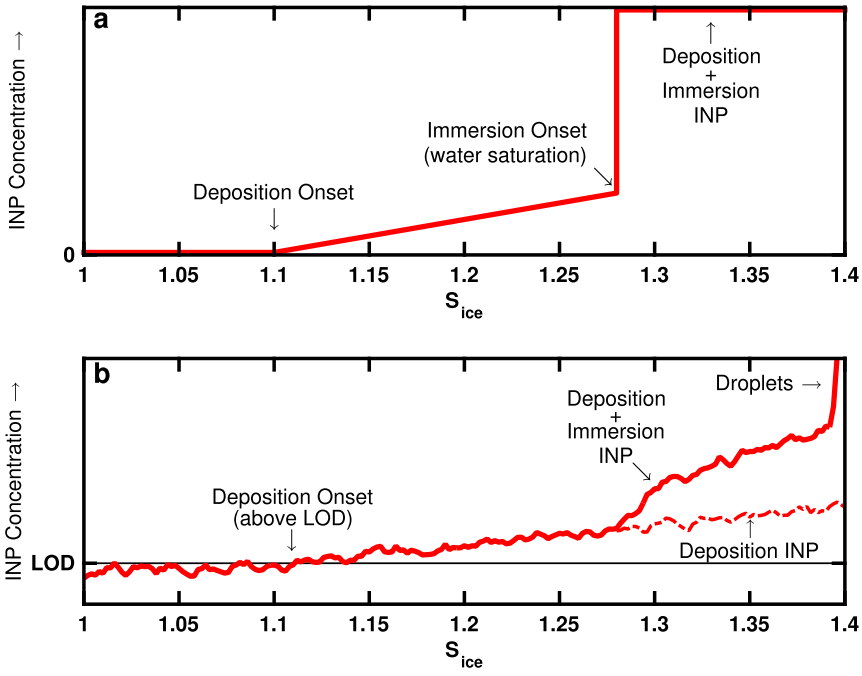

FIG. 1. Representation of (a) idealized and (b) realistic INP activation curves as a function of reported chamber S_{ice}. Curves assume a temperature of −25°C where liquid water saturation is at $S_{ice} \sim 1.28$ (Murphy and Koop 2005). The onset of deposition nucleation is assumed to be that of effective mineral dusts: $S_{ice} = 1.1$ (Hoose et al. 2008). The onset of immersion freezing is at water saturation (Pruppacher and Klett 1997). As noted in the text, reported CFDC data more closely resemble (b) than (a) (Garimella et al. 2016; DeMott et al. 2015).

and Earth's Radiant Energy System–Energy Balanced and Filled (CERES-EBAF) level 3B dataset (Loeb et al. 2009). Also considered are cases with fixed cf, as suggested by DeMott et al. (2015): cf = 0.1, 3, 4, 5, and 10 (cases 0.1B, 3B, 4B, 5B, and 10B, respectively). Note that DeMott et al. (2015) suggested cf = 3 for the CSU CFDC. Garimella et al. (2017) noted a mean cf = 4 using SPIN, a different CFDC, but also observed variability in cf that encompassed the range from ~1 to 10. Also note that cf = 0.1 does not correspond to a physical amount of particle spreading in a chamber (Garimella et al. 2017), but this case is included for completeness of the sensitivity analysis. To consider the effect of variability, a final case with stochastic cf values across the fixed range is considered (hereafter stoch). For the stoch case, the cf value for any given call to the ice nucleation scheme is randomly drawn from the measured distribution of cf values reported by Garimella et al. (2017).

Total aerosol indirect effects in the global climate model are diagnosed using the radiative flux perturbation (RFP) method (Haywood et al. 2009; Lohmann et al. 2010; Gettelman et al. 2012). The top-of-atmosphere radiative flux R is computed using two 6-yr simulations, one with present-day (PD; year 2000) aerosol and precursor emissions and another with preindustrial (PI; year 1850) emissions, and the RFP is given by $\mathrm{RFP} = R_{2000} - R_{1850}$. Both PD and PI runs have the same prescribed greenhouse gas and climatological sea surface temperature derived from the years 1980–2000. The changes in cloud forcing are decomposed into the changes in the shortwave cloud radiative forcing (SWCF) and longwave cloud radiative forcing (LWCF): $d\mathrm{SWCF} = \mathrm{SWCF}_{2000} - \mathrm{SWCF}_{1850}$ and $d\mathrm{LWCF} = \mathrm{LWCF}_{2000} - \mathrm{LWCF}_{1850}$. Additionally, the "clear sky" diagnostics recommended by Ghan (2013) are used to calculate cloud forcing correcting for the potential bias in "all-sky versus clear-sky" metrics that neglect the influence of above-cloud absorbing and below-cloud scattering aerosol.

The cloud-forcing response is related to changes in cloud microphysics and meteorological fields brought about by changes in INP concentrations. Since the only difference between the cases is the parameterization for het ice, we suggest that, since all other model configuration parameters are set to their default values (Kim et al. 2008, 2014), differences can be attributed to how a constant or variable low bias in INP parameterization can affect simulated cloud forcing.

3. Results

Figure 2 shows the PD LWCF and SWCF for the cases described in the previous section compared with the CERES-EBAF satellite observations.

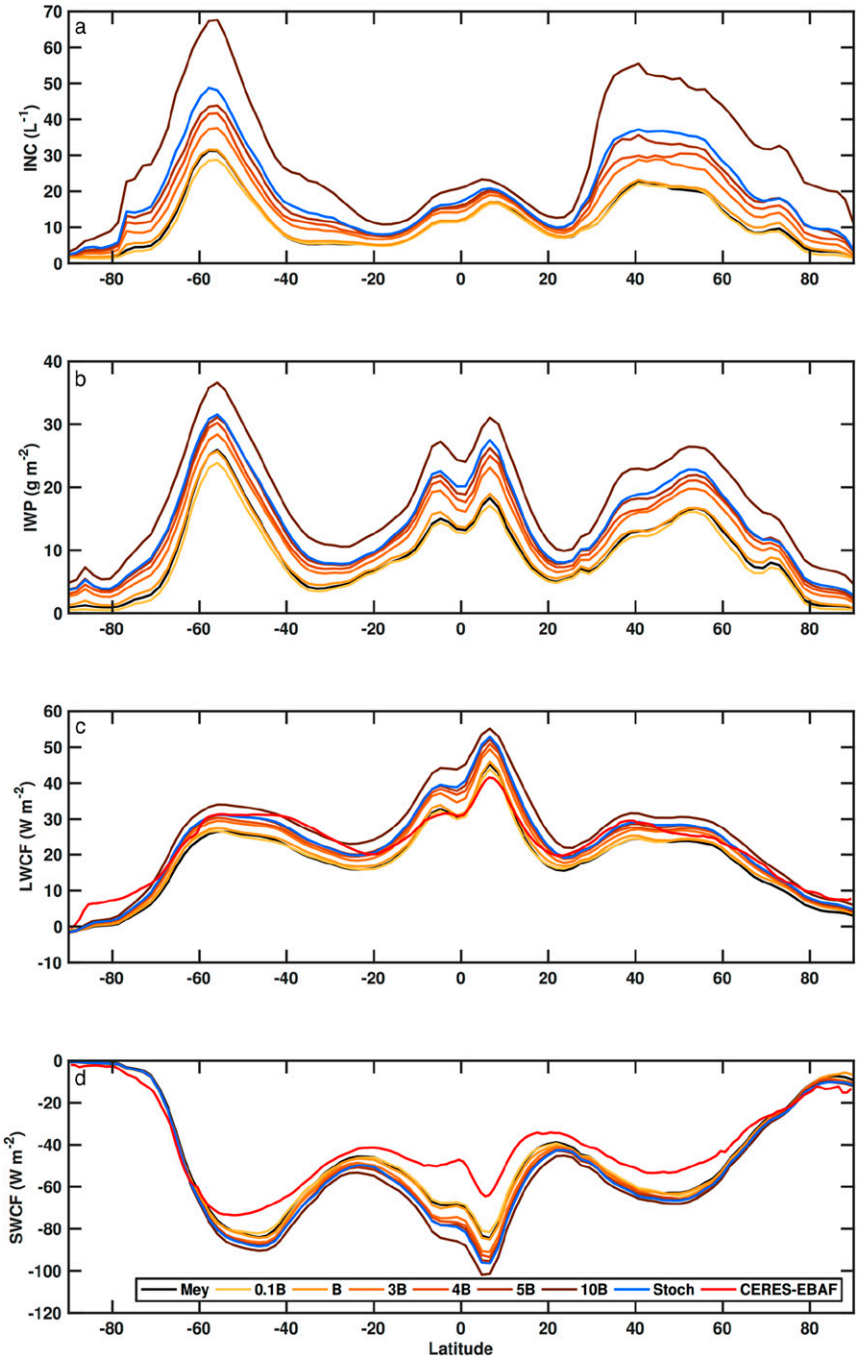

FIG. 2. Zonal averages of PD (a) INC, (b) IWP, (c) LWCF, and (d) SWCF for the cases described in the text and Table 1, as well as for (c),(d) CERES-EBAF satellite observations. Mey refers to the MEY parameterization INP. Case B is the parameterization by D10, and the prefix denotes a multiple (i.e., 3B is 3 times the INP of case B). Stoch refers to the stochastic INP concentration described in the text. For reference, the globally averaged LWCF and SWCF from the year 2000 CERES-EBAF observations are shown.

Table 1 shows globally averaged radiative and cloud properties in the PD and PI runs, the PD minus PI differences for LWCF and SWCF, ice water path (IWP), cloud-top ice number concentration (INC), cloud-top ice effective radius (REI), total cloud fraction (CLT), and cloud fraction at low (CLDLOW), medium (CLDMED), and high altitudes (CLDHGH). The table includes uncertainty estimates from bootstrapping 2-yr

TABLE 1. Radiative and cloud properties for each case in PD runs (top row in each set), in PI runs (middle row in each set), and the difference (bottom row in each set; see text for details) for LWCF, SWCF, IWP, INC, and REI. Average values for the final 5 out of 6 model years are shown. Mey and stoch are the MEY parameterization and stochastic cases described in the text, respectively. For reference, the globally averaged LWCF and SWCF from the year 2000 CERES-EBAF observations are 26.0 and −47.1 W m^{-2}, respectively.

		Mey	0.1B	B	3B	4B	5B	10B	Stoch
LWCF (W m^{-2})	PD	22.44 ± 0.03	22.43 ± 0.03	23.35 ± 0.03	25.64 ± 0.05	26.63 ± 0.01	27.46 ± 0.04	30.68 ± 0.06	27.70 ± 0.06
	PI	21.92 ± 0.04	21.75 ± 0.04	22.95 ± 0.05	25.63 ± 0.04	26.63 ± 0.04	27.60 ± 0.04	31.09 ± 0.14	27.93 ± 0.05
	Δ	0.52 ± 0.03	0.68 ± 0.05	0.40 ± 0.06	0.02 ± 0.02	0.00 ± 0.05	−0.14 ± 0.08	−0.41 ± 0.19	−0.23 ± 0.07
SWCF (W m^{-2})	PD	−55.36 ± 0.05	−55.29 ± 0.06	−56.38 ± 0.00	−58.71 ± 0.08	−59.81 ± 0.15	−60.60 ± 0.08	−63.67 ± 0.10	−60.87 ± 0.08
	PI	−53.21 ± 0.02	−52.96 ± 0.06	−54.16 ± 0.06	−57.02 ± 0.06	−57.93 ± 0.07	−59.05 ± 0.02	−62.31 ± 0.10	−59.30 ± 0.07
	Δ	−2.15 ± 0.04	−2.33 ± 0.05	−2.22 ± 0.07	−1.69 ± 0.05	−1.88 ± 0.20	−1.55 ± 0.08	−1.36 ± 0.16	−1.57 ± 0.03
IWP (g m^{-2})	PD	10.57 ± 0.04	9.87 ± 0.06	11.04 ± 0.04	13.47 ± 0.02	14.57 ± 0.03	15.51 ± 0.07	19.56 ± 0.05	16.02 ± 0.04
	PI	10.63 ± 0.05	9.91 ± 0.05	11.18 ± 0.03	13.83 ± 0.03	14.98 ± 0.03	16.00 ± 0.05	20.31 ± 0.14	16.61 ± 0.07
	Δ	−0.06 ± 0.07	−0.04 ± 0.10	−0.14 ± 0.06	−0.36 ± 0.02	−0.42 ± 0.05	−0.50 ± 0.12	−0.75 ± 0.18	−0.58 ± 0.08
LWP (g m^{-2})	PD	53.17 ± 0.08	55.53 ± 0.17	54.97 ± 0.06	56.17 ± 0.13	56.97 ± 0.27	57.16 ± 0.12	58.17 ± 0.22	57.22 ± 0.16
	PI	48.90 ± 0.15	50.92 ± 0.17	50.02 ± 0.20	51.92 ± 0.09	52.13 ± 0.22	52.72 ± 0.06	53.82 ± 0.12	52.67 ± 0.21
	Δ	4.26 ± 0.22	4.61 ± 0.23	4.96 ± 0.20	4.25 ± 0.04	4.85 ± 0.49	4.43 ± 0.06	4.35 ± 0.33	4.56 ± 0.24
INC (L^{-1})	PD	12.30 ± 0.12	11.82 ± 0.07	12.83 ± 0.16	15.99 ± 0.08	17.64 ± 0.13	19.25 ± 0.10	29.01 ± 0.20	20.63 ± 0.09
	PI	11.08 ± 0.13	10.81 ± 0.15	11.89 ± 0.08	14.81 ± 0.05	16.63 ± 0.11	18.65 ± 0.07	28.66 ± 0.26	20.07 ± 0.16
	Δ	1.22 ± 0.17	1.01 ± 0.21	0.94 ± 0.21	1.18 ± 0.13	1.01 ± 0.04	0.61 ± 0.17	0.35 ± 0.44	0.56 ± 0.14
REI (μm)	PD	13.99 ± 0.04	13.84 ± 0.02	14.06 ± 0.02	14.08 ± 0.05	14.12 ± 0.02	14.21 ± 0.04	14.36 ± 0.06	14.19 ± 0.03
	PI	14.33 ± 0.05	14.16 ± 0.08	14.35 ± 0.02	14.38 ± 0.02	14.41 ± 0.03	14.37 ± 0.04	14.49 ± 0.02	14.39 ± 0.03
	Δ	−0.34 ± 0.04	−0.31 ± 0.07	−0.29 ± 0.04	−0.29 ± 0.03	−0.28 ± 0.04	−0.17 ± 0.06	−0.13 ± 0.07	−0.21 ± 0.03
CLDTOT (%)	PD	41.78 ± 0.17	41.60 ± 0.03	41.92 ± 0.09	41.95 ± 0.05	42.25 ± 0.11	42.20 ± 0.06	42.36 ± 0.12	42.15 ± 0.06
	PI	41.64 ± 0.08	41.35 ± 0.05	41.58 ± 0.03	41.92 ± 0.06	41.93 ± 0.08	42.08 ± 0.06	42.29 ± 0.09	42.12 ± 0.04
	Δ	0.14 ± 0.14	0.26 ± 0.06	0.33 ± 0.08	0.02 ± 0.10	0.32 ± 0.05	0.12 ± 0.04	0.06 ± 0.20	0.04 ± 0.05
CLDLOW (%)	PD	27.07 ± 0.02	27.01 ± 0.06	27.39 ± 0.01	27.21 ± 0.03	27.26 ± 0.04	27.29 ± 0.04	27.33 ± 0.09	27.25 ± 0.01
	PI	26.87 ± 0.05	26.37 ± 0.08	27.08 ± 0.04	27.00 ± 0.04	27.00 ± 0.02	27.08 ± 0.08	27.10 ± 0.05	27.04 ± 0.04
	Δ	0.21 ± 0.05	0.64 ± 0.02	0.31 ± 0.03	0.21 ± 0.05	0.26 ± 0.02	0.21 ± 0.07	0.23 ± 0.11	0.21 ± 0.04
CLDMED (%)	PD	39.82 ± 0.14	40.56 ± 0.06	39.90 ± 0.08	40.47 ± 0.24	40.66 ± 0.06	41.04 ± 0.12	42.57 ± 0.12	41.16 ± 0.17
	PI	40.10 ± 0.14	40.90 ± 0.05	40.28 ± 0.08	40.70 ± 0.16	41.06 ± 0.12	41.47 ± 0.10	43.01 ± 0.16	41.71 ± 0.04
	Δ	−0.28 ± 0.11	−0.34 ± 0.01	−0.39 ± 0.16	−0.23 ± 0.14	−0.40 ± 0.15	−0.43 ± 0.20	−0.44 ± 0.24	−0.55 ± 0.18
CLDHGH (%)	PD	22.44 ± 0.03	22.43 ± 0.03	23.35 ± 0.03	25.64 ± 0.05	26.63 ± 0.01	27.46 ± 0.04	30.68 ± 0.06	27.70 ± 0.06
	PI	21.92 ± 0.04	21.75 ± 0.04	22.95 ± 0.05	25.63 ± 0.04	26.63 ± 0.04	27.60 ± 0.04	31.09 ± 0.14	27.93 ± 0.05
	Δ	0.52 ± 0.03	0.68 ± 0.05	0.40 ± 0.06	0.02 ± 0.02	0.00 ± 0.05	−0.14 ± 0.08	−0.41 ± 0.19	−0.23 ± 0.07

averages from the final 5 years of the 6-yr simulation. Bootstrapped samples are constructed from years 2 and 3, 3 and 4, 4 and 5, and 5 and 6 for the PD and PI runs, and the mean and standard deviations of these samples (as well as mean and standard deviations of the differences) are shown. The total cloud fraction tends to increase slightly as cf increases; this is driven by an increase in low clouds, which offsets a decrease in high clouds.

The cases with cf > 1 match globally averaged satellite values for PD LWCF more closely than the B or MEY cases, although there is large sensitivity of radiative and cloud properties to the version of the parameterization used. PD LWCF, IWP, INC, and REI increase as a function of fixed cf (with larger relative increases in IWP and INC than with REI), while PD SWCF decreases as a function of fixed cf. For the MEY case, PD and PI values are similar to those in the 0.1B and B cases. Different sensitivities to changing cf in the PD cases versus that in the PI cases lead to decreasing change in IWP (dIWP), decreasing dINC, and increasing dREI with increasing fixed cf. The value of dLWCF is positive in the MEY case and cases with smaller fixed cf but becomes negative at larger cf values. The value of dSWCF increases as a function of fixed cf. Overall, the choice of cf significantly affects the estimated dLWCF, which ranges over $\sim 0.8\,\mathrm{W\,m^{-2}}$ in the experimentally constrained cases (cf ≥ 1) and changes sign from positive to negative (Table 1; Fig. 3).

The values for radiative and cloud properties for the stoch case fall within the range of values from the largest fixed-cf cases. However, the changes in cloud properties and corresponding responses in radiative properties in the stoch case are significantly different than those from the 3B and 4B cases, despite all three having similar mean values of cf (Table 1). This difference is also apparent when comparing dLWCF to dIWP (Fig. 3). In particular, the stoch case exhibits more negative dIWP than the 3B and 4B cases and is one of the cases that exhibits a negative dLWCF. The differences between the stoch case and the 3B and 4B cases is also apparent in zonally averaged comparisons of dINC, dIWP, dLWCF, and dSWCF (Fig. 4), especially in the Northern Hemisphere.

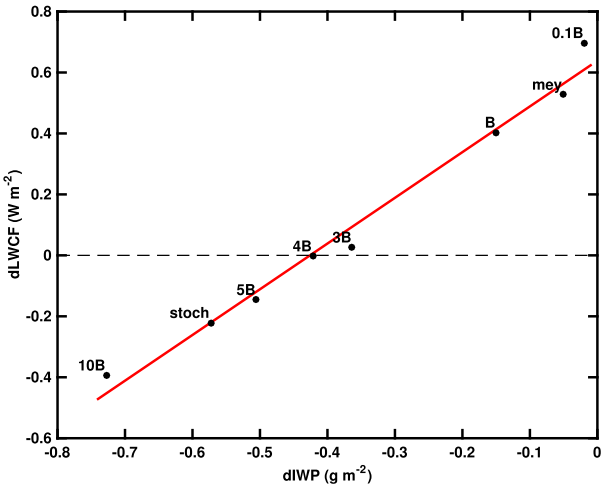

FIG. 3. Scatterplot of dLWCF vs dIWP for the cases described in the text and Table 1. A linear fit is given as the solid red line ($R^2 = 0.98$).

4. Discussion and conclusions

The results presented in the previous section indicate that the choice of cf significantly affects the estimated dLWCF. The PD value for LWCF increases with increasing fixed cf. There is similar behavior in PI LWCF values, but these exhibit more sensitivity to cf than the PD values, resulting in a negative dLWCF in the larger-cf cases. This cloud-forcing behavior coincides with changes in IWP. Both the PD and PI IWP values increase with increasing fixed cf. The sensitivity of IWP to cf is larger in the PI cases than in the PD cases, resulting in a decreasing dIWP as a function of fixed cf. Increasing cf but holding the emissions constant for either the PD or PI cases leads to an increase in cloud ice, but the increase is somewhat larger in the PI case. This suggests that in the PI case, when there are fewer aerosols overall, ice nucleation is more sensitive to small changes in the aerosol burden. This could lead to a "buffering" of ice formation as is thought to occur in aerosol–cloud interactions in the liquid phase (Stevens and Feingold 2009). Overall, there is a relatively smaller change in the amount of cloud ice in the PD cases compared to the PI cases for a given cf. This difference in sensitivity coincides with decreasing dLWCF with increasing fixed cf. At the largest cf values, this difference in sensitivity is most pronounced, and dLWCF decreases to the point at which it becomes negative.

These changes in longwave forcing arise from opposing cloud micro- and macrophysical processes. Increasing cf serves as a proxy for increasing the fraction of particles available to serve as INPs. Increasing this abundance of INPs only weakly impacts high-cloud coverage in the model but perturbs cloud microphysics by reducing the fractional change in ice water path, dIWP, as emissions increase. Traversing the cf parameter thus results in a regime change. When cf is small, ice clouds in the model exist in a regime where small positive aerosol perturbations only weakly influence cloud ice water and thus lead to a modest increase in LWCF. However, when cf is large, the same perturbation greatly

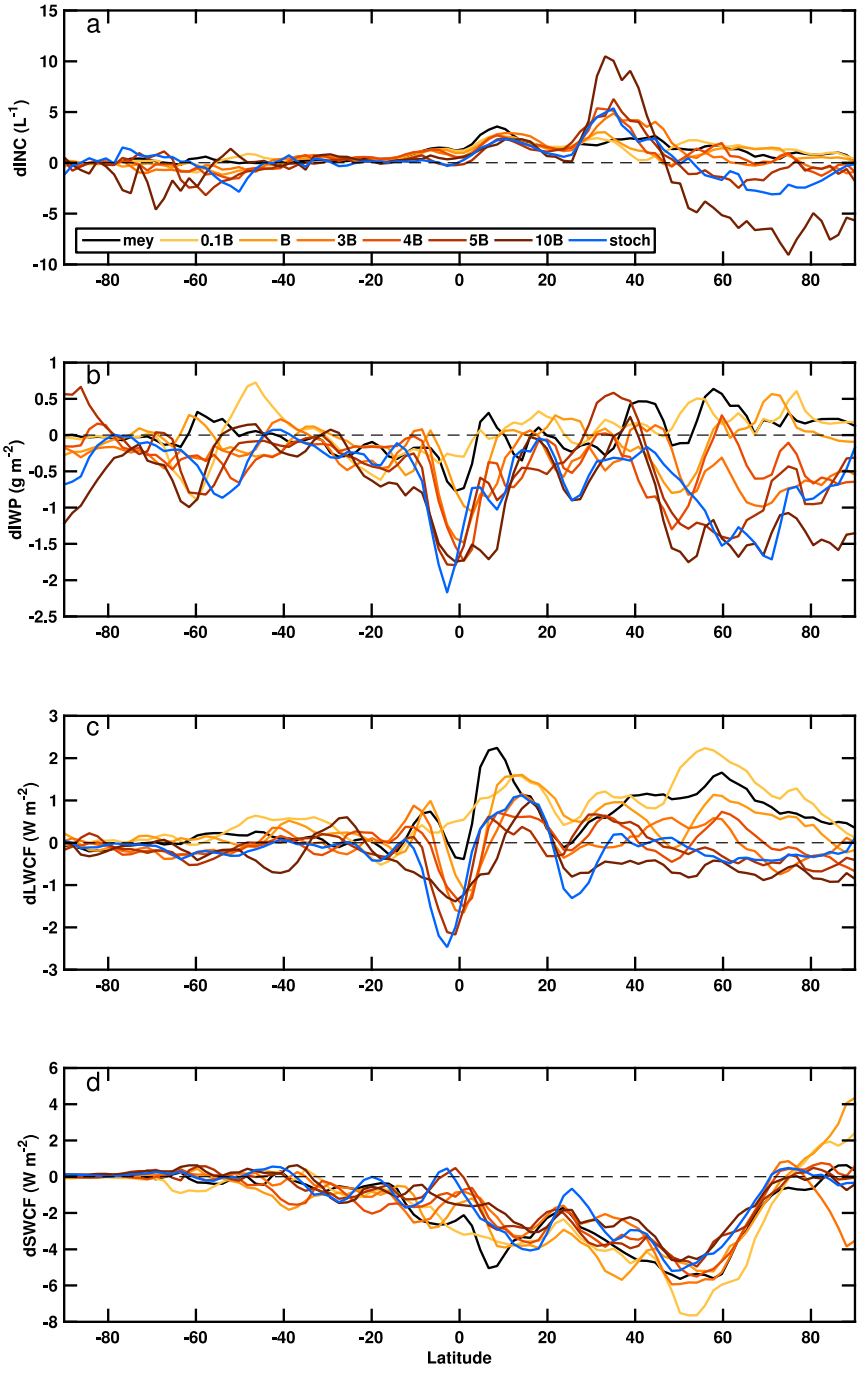

FIG. 4. Zonal averages of (a) *d*INC, (b) *d*IWP, (c) *d*LWCF and (d) *d*SWCF for the cases described in the text and Table 1. The notation follows that of Fig. 2. Mey refers to the MEY parameterization INP. Case B is the parameterization by D10, and the prefix denotes a multiple (i.e., 3B is 3 times the INP of the case B). Stoch refers to the stochastic INP concentration described in the text.

suppresses the development of cloud ice water and produces a small decline in LWCF.

The model results also suggest that there is a significant change in simulated cloud forcing when cf values are drawn from the distribution of measured values instead of being fixed. The model used in this study is particularly sensitive to ice-phase aerosol–cloud interactions when the number of potential ice nuclei is

very large; the stochastic parameterization here allows, infrequently, very large values of cf, which have a large impact on simulated cloud macrophysics and radiative forcing. Although the average cf drawn in the stochastic simulation here is close to 4, the simulation as a whole is quantitatively more similar to the case where cf > 5.

The cloud-forcing response is associated with changes in *d*INC, *d*REI, and *d*IWP. The relationship between cloud-property changes and radiative changes is similar to those reported in previous studies (e.g., Cziczo et al. 2009; Gettelman et al. 2012; Storelvmo et al. 2011; Xie et al. 2013): in particular, *d*INC and *d*IWP are positively correlated with *d*LWCF, but the exact relationship depends on the parameterization used. Furthermore, these results indicate that selecting the mean cf from a measured distribution does not produce the model response in *d*INC and *d*IWP and the corresponding changes in *d*LWCF that are produced from stochastic cf values, suggesting an influence of the tails of the cf distribution on model results.

These changes in INC and IWP are further associated with both cloud macrophysical changes (particularly low and high cloud fraction) and LWP. Within the model, increases in INC due to enhanced INP under present-day emissions or when cf is increased tend to produce more ice crystals. This does not necessarily produce higher IWP; as Gettelman et al. (2012) illustrate in their Table 3, given a simulation with sufficient background INC for given INP emissions, IWP can be suppressed as INP emissions are increased, as occurs when present-day emissions are used. This shifts the microphysical balance of mixed-phase processes toward liquid water, resulting in increases to LWP. More generally, these changes in emissions perturb the frequency and distribution of both liquid and ice water particles, which interact with ambient relative humidity in such a way to enhance cloud cover at low levels at the expense of high-level clouds.

Given these results, if heterogeneous ice nucleation parameterizations based on CFDC measurements are to be used extensively in the global modeling community, it is critical to account for both (i) the underprediction of INP in these observations and (ii) the variability (especially in the tails of the distribution) of INP measured with this technique. Small changes in these details, as shown here, can lead to different estimates of the background climatology of ice clouds and their sensitivity to aerosol perturbations, which can significantly alter the magnitude of aerosol impact on ice clouds within the same modeling framework.

These results also suggest that minimizing the uncertainty in estimates of this bias is an important step in constructing heterogeneous ice nucleation parameterizations based on CFDC measurements. Ideally, the value of cf would be inferred on a measurement-by-measurement basis and included when fitting parameterization constants: the sensitivity of the parameterization constants to uncertainty in the cf values could then also be quantified. Overall, in order to incorporate CFDC measurements in global models as a means of reducing the uncertainty that INP contribute to the climate system, both experimental and modeling efforts must carefully account for the variability in instrument bias and consider the uncertainty associated with it.

Acknowledgments. The authors gratefully acknowledge funding from NASA Grant NNX13AO15G and NSF Grant AGS-1339264. The source code for MARC as used in this work, version 1.0.2, is archived online (https://doi.org/10.5281/zenodo.168192). We thank NCAR's Computational and Information Systems Laboratory for the Educational Computing Allocation (UMIT0013). We would also like to thank Alexander Avramov for the useful discussions.

REFERENCES

Boose, Y., and Coauthors, 2016: Ice nucleating particles in the Saharan air layer. *Atmos. Chem. Phys.*, **16**, 9067–9087, https://doi.org/10.5194/acp-16-9067-2016.

Boucher, O., and Coauthors, 2013: Clouds and aerosols. *Climate Change 2013: The Physical Science Basis*, T. F. Stocker et al., Eds., Cambridge University Press, 571–657, https://doi.org/10.1017/CBO9781107415324.016.

Chou, C., O. Stetzer, E. Weingartner, Z. Juranyi, Z. A. Kanji, and U. Lohmann, 2011: Ice nuclei properties within a Saharan dust event at the Jungfraujoch in the Swiss Alps. *Atmos. Chem. Phys.*, **11**, 4725–4738, https://doi.org/10.5194/acp-11-4725-2011.

Cziczo, D. J., and Coauthors, 2009: Inadvertent climate modification due to anthropogenic lead. *Nat. Geosci.*, **2**, 333–336, https://doi.org/10.1038/ngeo499.

DeMott, P. J., D. J. Cziczo, A. J. Prenni, D. M. Murphy, S. M. Kreidenweis, D. S. Thomson, R. Borys, and D. C. Rogers, 2003a: Measurements of the concentration and composition of nuclei for cirrus formation. *Proc. Natl. Acad. Sci. USA*, **100**, 14 655–14 660, https://doi.org/10.1073/pnas.2532677100.

——, K. Sassen, M. R. Poellot, D. Baumgardner, D. C. Rogers, S. D. Brooks, A. J. Prenni, and S. M. Kreidenweis, 2003b: African dust aerosols as atmospheric ice nuclei. *Geophys. Res. Lett.*, **30**, 1732, https://doi.org/10.1029/2003GL017410.

——, and Coauthors, 2010: Predicting global atmospheric ice nuclei distributions and their impacts on climate. *Proc. Natl. Acad. Sci. USA*, **107**, 11 217–11 222, https://doi.org/10.1073/pnas.0910818107.

——, and Coauthors, 2015: Integrating laboratory and field data to quantify the immersion freezing ice nucleation activity of mineral dust particles. *Atmos. Chem. Phys.*, **15**, 393–409, https://doi.org/10.5194/acp-15-393-2015.

Fan, J., and Coauthors, 2014: Aerosol impacts on California winter clouds and precipitation during CalWater 2011: Local pollution versus long-range transported dust. *Atmos. Chem. Phys.*, **14**, 81–101, https://doi.org/10.5194/acp-14-81-2014.

Forster, P., and Coauthors, 2007: Changes in atmospheric constituents and in radiative forcing. *Climate Change 2007: The Physical Science Basis*, S. Solomon et al., Eds., Cambridge University Press, 747–845.

Garimella, S., and Coauthors, 2016: The Spectrometer for Ice Nuclei (SPIN): An instrument to investigate ice nucleation. *Atmos. Meas. Tech.*, **9**, 2781–2795, https://doi.org/10.5194/amt-9-2781-2016.

——, D. A. Rothenberg, M. J. Wolf, R. O. David, Z. A. Kanji, C. Wang, M. Rösch, and D. J. Cziczo, 2017: Uncertainty in counting ice nucleating particles with continuous flow diffusion chambers. *Atmos. Chem. Phys.*, **17**, 10 855–10 864, https://doi.org/10.5194/acp-17-10855-2017.

Gettelman, A., X. Liu, D. Barahona, U. Lohmann, and C. C. Chen, 2012: Climate impacts of ice nucleation. *J. Geophys. Res.*, **117**, D20201, https://doi.org/10.1029/2012JD017950.

——, H. Morrison, S. Santos, P. Bogenschutz, and P. Caldwell, 2015: Advanced two-moment bulk microphysics for global models. Part II: Global model solutions and aerosol–cloud interactions. *J. Climate*, **28**, 1288–1307, https://doi.org/10.1175/JCLI-D-14-00103.1.

Ghan, S. J., 2013: Technical note: Estimating aerosol effects on cloud radiative forcing. *Atmos. Chem. Phys.*, **13**, 9971–9974, https://doi.org/10.5194/acp-13-9971-2013.

Hande, L. B., C. Engler, C. Hoose, and I. Tegen, 2015: Seasonal variability of Saharan desert dust and ice nucleating particles over Europe. *Atmos. Chem. Phys.*, **15**, 4389–4397, https://doi.org/10.5194/acp-15-4389-2015.

Haywood, J. M., L. J. Donner, A. Jones, and J.-C. Golaz, 2009: Global indirect radiative forcing caused by aerosols: IPCC (2007) and beyond. *Clouds in the Perturbed Climate System: Their Relationship to Energy Balance, Atmospheric Dynamics, and Precipitation*, J. Heintzenberg and R. J. Charlson, Eds., MIT Press, 451–467.

Hoose, C., U. Lohmann, R. Erdin, and I. Tegen, 2008: The global influence of dust mineralogical composition on heterogeneous ice nucleation in mixed-phase clouds. *Environ. Res. Lett.*, **3**, 025003, https://doi.org/10.1088/1748-9326/3/2/025003.

Kim, D., C. Wang, A. Ekman, M. Barth, and P. Rasch, 2008: Distribution and direct radiative forcing of carbonaceous and sulfate aerosols in an interactive size-resolving aerosol–climate model. *J. Geophys. Res.*, **113**, D16309, https://doi.org/10.1029/2007JD009756.

——, ——, ——, ——, and D. Lee, 2014: The responses of cloudiness to the direct radiative effect of sulfate and carbonaceous aerosols. *J. Geophys. Res. Atmos.*, **119**, 1172–1185, https://doi.org/10.1002/2013JD020529.

Koop, T., B. Luo, A. Tsias, and T. Peter, 2000: Water activity as the determinant for homogeneous ice nucleation in aqueous solutions. *Nature*, **406**, 611–614, https://doi.org/10.1038/35020537.

Lau, K. M., and H. T. Wu, 2007: Detecting trends in tropical rainfall characteristics, 1979–2003. *Int. J. Climatol.*, **27**, 979–988, https://doi.org/10.1002/joc.1454.

Liu, X., and J. Penner, 2005: Ice nucleation parameterization for global models. *Meteor. Z.*, **14**, 499–514, https://doi.org/10.1127/0941-2948/2005/0059.

Loeb, N., B. Wielicki, D. Doelling, G. Smith, D. Keyes, S. Kato, N. Manalo-Smith, and T. Wong, 2009: Toward optimal closure of the Earth's top-of-atmosphere radiation budget. *J. Climate*, **22**, 748–766, https://doi.org/10.1175/2008JCLI2637.1.

Lohmann, U., and Coauthors, 2010: Total aerosol effect: Radiative forcing or radiative flux perturbation? *Atmos. Chem. Phys.*, **10**, 3235–3246, https://doi.org/10.5194/acp-10-3235-2010.

Lynch, D. K., K. Sassen, D. O. Starr, and G. Stephens, 2002: *Cirrus*. Oxford University Press, 504 pp.

Meyers, M. P., P. J. DeMott, and W. R. Cotton, 1992: New primary ice nucleation parameterizations in an explicit cloud model. *J. Appl. Meteor.*, **31**, 708–721, https://doi.org/10.1175/1520-0450(1992)031<0708:NPINPI>2.0.CO;2.

Murphy, D. M., and T. Koop, 2005: Review of the vapour pressures of ice and supercooled water for atmospheric applications. *Quart. J. Roy. Meteor. Soc.*, **131**, 1539–1565, https://doi.org/10.1256/qj.04.94.

Murray, B. J., D. O'Sullivan, J. D. Atkinson, and M. E. Webb, 2012: Ice nucleation by particles immersed in supercooled cloud droplets. *Chem. Soc. Rev.*, **41**, 6519–6554, https://doi.org/10.1039/c2cs35200a.

Neale, R. B., and Coauthors, 2010: Description of the NCAR Community Atmosphere Model (CAM5.0). NCAR Tech. Note NCAR/TN-486+STR, 268 pp., www.cesm.ucar.edu/models/cesm1.1/cam/docs/description/cam5_desc.pdf.

Pruppacher, H. R., and J. D. Klett, 1997: *Microphysics of Clouds and Precipitation.* 2nd ed. Kluwer Academic, 954 pp.

Rogers, D. C., 1988: Development of a continuous flow thermal gradient diffusion chamber for ice nucleation studies. *Atmos. Res.*, **22**, 149–181, https://doi.org/10.1016/0169-8095(88)90005-1.

Stetzer, O., B. Baschek, F. Lüönd, and U. Lohmann, 2008: The Zurich Ice Nucleation Chamber (ZINC)—A new instrument to investigate atmospheric ice formation. *Aerosol Sci. Technol.*, **42**, 64–74, https://doi.org/10.1080/02786820701787944.

Stevens, B., and G. Feingold, 2009: Untangling aerosol effects on clouds and precipitation in a buffered system. *Nature*, **461**, 607–613, https://doi.org/10.1038/nature08281.

Storelvmo, T., C. Hoose, and P. Eriksson, 2011: Global modeling of mixed-phase clouds: The albedo and lifetime effects of aerosols. *J. Geophys. Res.*, **116**, D05207, https://doi.org/10.1029/2010JD014724.

Tan, I., and T. Storelvmo, 2016: Sensitivity study on the influence of cloud microphysical parameters on mixed-phase cloud thermodynamic phase partitioning in CAM5. *J. Atmos. Sci.*, **73**, 709–728, https://doi.org/10.1175/JAS-D-15-0152.1.

Tobo, Y., and Coauthors, 2013: Biological aerosol particles as a key determinant of ice nuclei populations in a forest ecosystem. *J. Geophys. Res. Atmos.*, **118**, 10 100–10 110, https://doi.org/10.1002/jgrd.50801.

Wex, H., and Coauthors, 2014: Kaolinite particles as ice nuclei: Learning from the use of different kaolinite samples and different coatings. *Atmos. Chem. Phys.*, **14**, 5529–5546, https://doi.org/10.5194/acp-14-5529-2014.

Xie, S., X. Liu, C. Zhao, and Y. Zhang, 2013: Sensitivity of CAM5-simulated Arctic clouds and radiation to ice nucleation parameterization. *J. Climate*, **26**, 5981–5999, https://doi.org/10.1175/JCLI-D-12-00517.1.